Separation and Purification Technology 77 (2011) 251–260

Separation and Purification Technology

journal homepage: www.elsevier.com/locate/seppur

Dynamic bed measurements of CO adsorption on microporous adsorbents at high pressures for hydrogen purification processes

M. Bastos-Neto[a], A. Moeller[a], R. Staudt[b,*], J. Böhm[c], R. Gläser[a,c]

[a] Institut für Nichtklassische Chemie e.V., Permoserstr. 15, 04318 Leipzig, Germany
[b] Fakultät Maschinenbau und Verfahrenstechnik (M+V), Hochschule Offenburg, Badstraße 24, 77652 Offenburg, Germany
[c] Institut für Technische Chemie, Universität Leipzig, Linnéstr. 3, 04103 Leipzig, Germany

ARTICLE INFO

Article history:
Received 1 October 2010
Received in revised form 7 December 2010
Accepted 10 December 2010

Keywords:
Adsorption
Fixed bed
Simulation
Modeling
Separation
Hydrogen purification
Carbon monoxide

ABSTRACT

Regarding the importance of adsorptive removal of carbon monoxide from hydrogen-rich mixtures for novel applications (e.g. fuel cells), this work provides a series of experimental data on adsorption isotherms and breakthrough curves of carbon monoxide. Three recently developed 5A zeolites and one commercial activated carbon were used as adsorbents. Isotherms were measured gravimetrically at temperatures of 278–313 K and pressures up to 0.85 MPa. Breakthrough curves of CO were obtained from dynamic column measurements at temperatures of 298–301 K, pressures ranging from 0.1 MPa to ca. 6 MPa and concentrations of CO in H_2/CO mixtures of 5–17.5 mol%. A simple mathematical model was developed to simulate breakthrough curves on adsorbent beds using measured and calculated data as inputs. The number of parameters and the use of correlations to evaluate them were restricted in order to focus the importance of measured values. For the given assumptions and simplifications, the results show that the model predictions agree satisfactorily with the experimental data at the different operating conditions applied.

1. Introduction

In spite of not being a primary energy source hydrogen needs to be produced and consequently purified. The current main source of hydrogen is the processing of fossil derivates like methane, coal and heavy hydrocarbons. Other sources include electrolysis and biological processes [1–3].

The most common and economical way to produce hydrogen is through steam reforming of natural gas combined with a water–gas shift reaction, from which a hydrogen-rich stream (70–80%) containing impurities, namely hydrogen sulfide (traces), water vapor (<1%), nitrogen (<1%), methane (3–6%), carbon monoxide (1–3%) and carbon dioxide (15–25%), is produced [4–6]. In order to obtain hydrogen with the desired purity these contaminants must be removed. The removal process is industrially carried out by pressure swing adsorption (PSA), which is usually designed to obtain a hydrogen stream containing 98–99.999 mol% H_2 [6,7].

In practice, PSA units for hydrogen purification use up to three different adsorbent layers. The first layer reached by the feed mixture, usually a guard bed, is composed of alumina or silica gel to essentially adsorb H_2O; the second is composed of activated carbon, which adsorbs CH_4, CO, CO_2 and traces of sulfur components; and as a third layer, zeolites are used for improved adsorption of CO, N_2 and other trace components [8,9]. Therefore, factors like the choice of material, the relative length (ratio) of the layers, composition of the feed gas and interactions gas–solid can significantly influence the yield and efficiency of the process [5,8–10].

Despite the remarkable growth in practical applications of adsorptive gas separation, the commercial design and optimization of these processes still largely remain an experimental effort. This is primarily due to the inherent complex nature of the practical adsorption systems [11].

The most important challenges in this area today are (i) a deeper understanding of the equilibrium, the dynamics and thermal effects involved in the separation of mixtures; and (ii) the development of less expensive and less time-consuming models to describe the influence of the equilibrium, kinetics and heat effects on such processes. Today's models frequently cannot predict data with the accuracy and reliability required by industry [11–13]. A more detailed covering of the contemporary research needs with interesting examples of the current industrial design requirements can be found elsewhere [11].

To achieve the desired reliability of the model it is necessary to have a considerable amount of experimental data, including mainly

Abbreviations: AC, activated carbon; PSA, pressure swing adsorption; SATP, Standard Ambient Temperature and Pressure (25 °C and 100.000 kPa).

* Corresponding author. Tel.: +49 0341 235 2405; fax: +49 0341 235 2701.
E-mail address: Reiner.Staudt@fh-offenburg.de (R. Staudt).

1383-5866 © 2010 Elsevier B.V. Open access under the Elsevier OA license.
doi:10.1016/j.seppur.2010.12.015

Nomenclature

A	bed sectional area (m^2)
$C_{g,i}$	component concentration in the gas phase ($mol\,kg^{-1}$)
$\tilde{c}_{pg,i}$	component molar specific heat at constant pressure ($J\,mol^{-1}\,K^{-1}$)
$\hat{c}_{ps}$	particle specific heat at constant pressure ($J\,kg^{-1}\,K^{-1}$)
$\hat{c}_{pw}$	wall specific heat at constant pressure ($J\,kg^{-1}\,K^{-1}$)
D_{ax}	axial mass dispersion coefficient ($m^2\,s^{-1}$)
d_i	column internal diameter (m)
D_m	molecular diffusivity ($m^2\,s^{-1}$)
e_w	wall thickness (m)
h_w	film heat transfer coefficient between the gas and wall ($W\,m^{-2}\,K^{-1}$)
k_{eff}	effective mass transfer coefficient (s^{-1})
k_g	gas thermal conductivity ($W\,m^{-1}\,K^{-1}$)
K_i	Toth isotherm parameter – "affinity"
$K_{0,i}$	affinity at reference temperature T_0
L	bed length (m)
m_E	adsorbent mass (kg)
n_i	Toth heterogeneity parameter
$n_{0,i}$	heterogeneity parameter at reference temperature T_0
p	total pressure (MPa)
$\bar{q}_i$	component average concentration on the adsorbed phase ($mol\,kg^{-1}$)
Q_i	heat of adsorption for fractional loading equal to zero ($J\,mol^{-1}$)
q_i^*	adsorbed concentration in equilibrium with $C_{g,i}$ ($mol\,kg^{-1}$)
$q_{max,i}$	Toth isotherm parameter – maximal concentration ($mol\,kg^{-1}$)
$q_{max0,i}$	maximum adsorbed amount at reference temperature T_0 ($mol\,kg^{-1}$)
R	ideal gas constant ($J\,mol^{-1}\,K^{-1}$)
R^2	coefficient of determination for the isotherm model fitting
r_p	average particle radius (m)
t	time (s)
T_∞	room temperature (K)
T_0	reference temperature for isotherm fitting (K)
T	bulk phase temperature (K)
T_w	wall temperature (K)
u	advection (interstitial) velocity ($m\,s^{-1}$)
U_g	overall heat transfer coefficient ($W\,m^{-2}\,K^{-1}$)
y_i	component molar fraction
z	axial position (m)
ΔH_i	isosteric heat of adsorption for component i ($J\,mol^{-1}$)
α_w	ratio of the internal surface area to the volume of the column wall (m^{-1})
α_{wL}	ratio of the log mean surface to the volume of column wall (m^{-1})
ε	bed porosity
ε_p	particle porosity
θ	fractional loading ($\theta = q_i^*/q_{max,i}$)
κ_i	parameter for the temperature dependency of the Toth exponent
ρ	fluid density ($kg\,m^{-3}$)
ρ_{ap}	particle average density ($kg\,m^{-3}$)
ρ_w	wall density ($kg\,m^{-3}$)
χ_i	the coefficient for the temperature dependency of the maximum capacity

adsorption isotherms and breakthrough curves, which can provide a direct and realistic interpretation of the adsorption process. By measuring breakthrough curves, one can evaluate the amount adsorbed, the influence of other species and the interval required by each step (adsorption–desorption).

Most of the available data on breakthrough curves of CH_4, CO, CO_2 and N_2 in hydrogen are results of simulations, mainly those at high pressures (above 2.0 MPa), providing few experimental data. The current literature lacks measured data at different pressure and temperature conditions, especially in newly developed materials [12,13].

Carbon monoxide was chosen as a component to be removed from H_2-rich mixtures for this study, since only few experimental data are available from the literature and the importance of its concentration on H_2 for fuel cells applications. CO tends to act as a severe poison towards the platinum catalyst in a PEM fuel cell and for this reason its concentration must be generally reduced to levels as low as 10 ppm [14].

The main goal of this study was to provide a series of experimental data for breakthrough curves and adsorption isotherms of CO on different materials, including an activated carbon and new commercial zeolites, with different feed compositions and pressures ranging from 0.1 to 6 MPa. Then, a simple model was applied using measured parameters (obtained from adsorption isotherms, bed geometry, etc.) and properties evaluated according to corresponding literature data, for instance heat capacity and conductivity, as input values. After that, this model was validated by comparing simulations with experiments.

With the modeling and experimental investigation, this study also aimed a deeper insight into the adsorptive separation of carbon monoxide from hydrogen on fixed beds, by analyzing the influence of the adsorption equilibrium and operational variables such as the feed flow rate, pressure and composition on the performance of a separation unit.

2. Model

In this section we provide a simple approach to the calculation of fixed bed adsorption. A comprehensive summary of models developed to analyze data and predict results for a variety of adsorption systems has been reported in the literature [15].

In order to describe the dynamic behavior of separation processes in fixed beds a general mathematical model was used, which consists of the coupled mass and energy balances with suitable boundary and initial conditions. The set of differential equations was solved by numerical integration using the Euler method, written in Borland Delphi 3.0. The model was designed based on the system schematically illustrated in Fig. 1 with assumptions commonly found in the literature [4,16–19] and simplified for reasons to be discussed below.

2.1. Model assumptions

1. Ideal gas behavior of the adsorptive throughout the column.
2. No mass, heat or velocity gradients in the radial direction.
3. Plug flow with axial mass dispersion.
4. Negligible external mass transfer effect (i.e. film mass transfer and macropore diffusion).
5. Mass transfer into the particle described according to the linear driving force (LDF) model [7,16,19].
6. No temperature gradient inside the particles and thermal equilibrium between the gas and the adsorbent.
7. The system is assumed to operate adiabatically.
8. Constant heat transfer coefficients.
9. Constant and homogeneous bed porosity along the bed length.

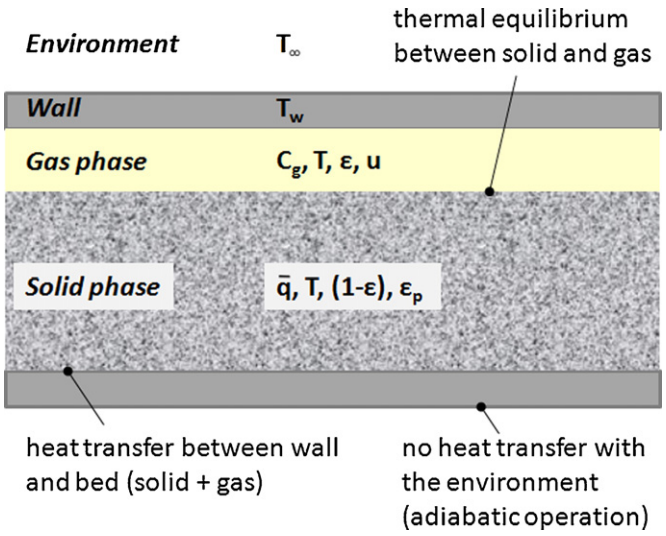

Fig. 1. Schematic representation of the fixed bed.

10. No pressure drop was considered.

2.2. Model equations and parameters

As no radial dispersion is considered and the volumetric flow rate remains constant along the bed ($\partial u/\partial t = 0$), the mass balance can be written as follows:

$$\frac{\partial C_{g,i}}{\partial t} + u\frac{\partial C_{g,i}}{\partial z} - D_{ax}\frac{\partial^2 C_{g,i}}{\partial z^2} + \frac{(1-\varepsilon)}{\varepsilon}\left(\varepsilon_p\frac{\partial C_{g,i}}{\partial t} + \rho_{ap}\frac{\partial \bar{q}_i}{\partial t}\right) = 0 \quad (1)$$

The ideal gas law is used to correlate the partial pressures to the concentrations:

$$p = R\cdot T\sum_i C_{g,i} \quad (2)$$

Ignoring the external mass transfer effect and using the LDF approximation for intra-pellet diffusion, the rate in which the average concentration changes is expressed as follows:

$$\frac{\partial \bar{q}_i}{\partial t} = k_{eff}\cdot(q_i^* - \bar{q}_i) \quad (3)$$

The effective mass transfer coefficient, k_{eff}, was assumed to be constant for a given operation and fitted to each breakthrough curve.

The assumption of thermal equilibrium between gas and adsorbent in each axial position is reported to be very reasonable [4]. Additionally, no dispersive energy transfer is taken into account. Another simplification is that the adsorbed phase heat capacity is negligible [16], as its magnitude is much lower than the sum of the other heat capacities (fluid phase, adsorbent and wall). Hence, we have two energy balances:

$$\sum_i (C_{g,i}\cdot\tilde{c}_{pg,i})\cdot u\frac{\partial T}{\partial z} + \left(\sum_i (C_{g,i}\cdot\tilde{c}_{vg,i}) + \frac{1-\varepsilon}{\varepsilon}\rho_{ap}\hat{c}_s\right)\frac{\partial T}{\partial t} + \frac{4h_w}{\varepsilon d_i}(T-T_w) + \frac{1-\varepsilon}{\varepsilon}\rho_{ap}\sum_i\left(-\Delta H_i\frac{\partial \overline{q_i}}{\partial t}\right) = 0 \quad (4)$$

and

$$\rho_w\hat{c}_{pw}\frac{\partial T_w}{\partial t} = \alpha_w h_w(T-T_w) - \alpha_{wL}U_g(T_w - T_\infty) \quad (5)$$

where α_w and α_{wL} are geometrical factors (see nomenclature) and the overall heat transfer coefficient, U_g, is set to zero (adiabatic system).

The adsorption equilibrium was described by the Toth model:

$$q_i^* = q_{\max,i}\frac{K_i C_{g,i}}{(1+(K_i C_{g,i})^{n_i})^{1/n_i}} \quad (6)$$

The temperature dependence of K, $q_{\max,i}$ and n_i was evaluated according to Do [21] as described below:

$$K_i = K_{0,i}\exp\left(\frac{Q_i}{R}\left(\frac{1}{T}-\frac{1}{T_0}\right)\right) \quad (7)$$

$$q_{\max,i} = q_{\max 0,i}\exp\left(\chi_i\left(1-\frac{T}{T_0}\right)\right) \quad (8)$$

$$n_i = n_{0,i} + \kappa_i\left(1-\frac{T_0}{T}\right) \quad (9)$$

The axial mass dispersion coefficient was calculated as described in Ref. [22] using the following correlation:

$$D_{ax} = (0.45 + 0.55\varepsilon)D_m + 0.35 r_p u \quad (10)$$

where D_m, the molecular diffusivity, was calculated for each experimental run at feed temperature and pressure conditions using the Chapman–Enskog equation [23].

Heat capacities of H_2 and CO were evaluated with a polynomial function of the temperature [24] and the heat capacity of the mixture was calculated as follows:

$$\tilde{c}_{pg} = \sum_i(\tilde{c}_{pg,i}y_i) \quad (11)$$

The film heat transfer coefficient between the gas and wall, h_w, was calculated according to the following equation:

$$h_w = \frac{Nu\cdot k_g}{d_i} \quad (12)$$

The Nusselt number, Nu, was set to 5.77, which corresponds to plug flow with constant wall temperature in a circular tube [23] and the gas mixture thermal conductivity, k_g, was calculated as reported in Refs. [23,24] at feed conditions and assumed to be constant along the bed operation.

The following boundary and initial conditions were used:

$$C_{g,i}(z=0,t) = \frac{D_{ax}}{u}\frac{\partial C_{g,i}}{\partial z} + C_0$$
$$C_{g,i}(z>0,t=0) = 0$$
$$\left.\frac{\partial C_{g,i}}{\partial z}\right|_{z=L} = 0$$

$$T(z=0,t) = T_0$$
$$T(z>0,t=0) = T_0$$
$$\left.\frac{\partial T}{\partial z}\right|_{z=L} = 0$$

The boundary and initial conditions define an empty adsorber, which is thermally equilibrated with the environment at the beginning, with no concentration and temperature gradients within the bed outlet. The well known Dankwerts boundary condition was applied at the inlet of the adsorber to consider the effects of dispersion on the concentration.

The model parameters were analyzed for the relative sensitivity on the process dynamics and influence on the simulation. Model validation was accomplished by comparing simulations with the experimental data.

3. Materials and methods

Hydrogen (99.9992%) and carbon monoxide (99.997%), used in this study, were supplied by Air Products (Germany). The used adsorbents were three zeolites 5A, namely zeolite A and zeolite B

Table 1
Textural characteristics of the samples.

Sample	Specific surface area [$m^2\ g^{-1}$]	Total pore volume [$cm^3\ g^{-1}$]	Average pore size [nm]
AC D55/2 C PSA	765.4	0.414	0.54
Zeolite A	669.9	0.274	0.41
Zeolite B	669.9	0.282	0.42
KÖSTROLITH 5ABF	680.0	0.279	0.41

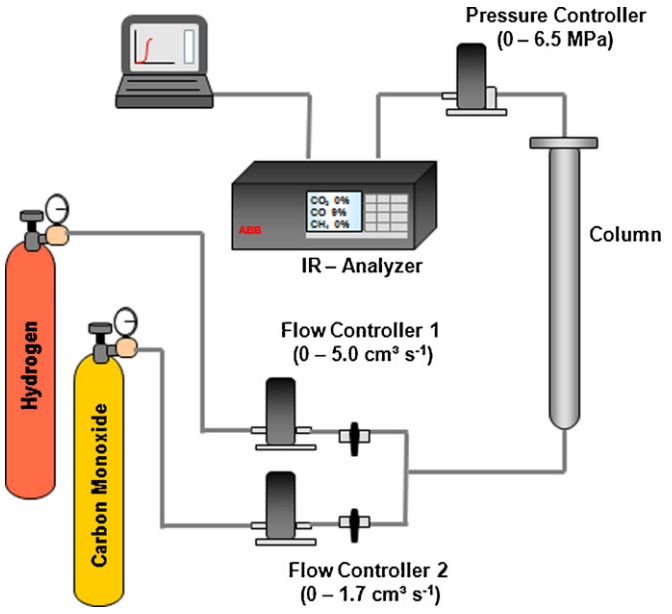

Fig. 2. Illustration of the experimental system for the measurement of breakthrough curves.

provided by Mahler AGS GmbH (Germany) and KÖSTROLITH 5ABF (binder-free) produced by CWK Chemiewerk Bad Köstritz GmbH (Germany) and one activated carbon sample, AC D55/2 C PSA, manufactured by CarboTech AC GmbH (Germany), all of them assumed to be suitable for H_2 purification processes. Textural characteristics of the samples, evaluated through N_2 isotherms at 77 K, are shown in Table 1.

The experimental setup for measuring breakthrough curves, represented in Fig. 2, consists of a stainless steel column, where the adsorbent sample was packed; two mass flow controllers (max. flow of 5.0 $cm^3\ s^{-1}$ (SATP) and 1.7 $cm^3\ s^{-1}$ (SATP)); a pressure controller (max. 6.5 MPa) from Brooks Instrument (USA); and a continuous gas analyzer with an Infra-Red detector from ABB – Hartmann & Braun (Germany).

The adsorbent bed was tested for the capacity and kinetics of CO adsorption by measuring breakthrough curves at distinct pressures and concentrations. Table 2 lists the column characteristics and physical properties of the adsorbents and Table 3 shows the operating conditions of each experimental run for all adsorbent samples.

The regeneration conditions were 5 h at 423 K for the activated carbon sample and about 10 h at 673 K for the zeolites, in both cases with approximately 1.0 $cm^3\ s^{-1}$ (SATP) helium flow. Subsequently, the bed was purged with pure hydrogen for at least 30 min to assure the absence of helium during the experiments. After the regeneration step, cyclic experiments (2–4 cycles) were carried out for a given concentration and pressure at room temperature. Feed concentrations of mixtures H_2/CO were set by adjusting the gas flow controllers. Between each cycle, there was a desorption step to purge the bed with pure H_2 at the same flow rate used in the adsorption step, accomplished by closing the CO-stream valve after bed saturation.

Adsorption isotherms were measured with a magnetic suspension balance from Rubotherm (Germany) and evaluated according to literature Refs. [20,21,25–29].

4. Results and discussions

In industrial separation units the adsorbent column is usually filled with a carbon layer, the first to be percolated by the mixture, and a zeolite layer. Part of the CO is retained in the carbon bed and the rest breaks through it to the zeolite bed. The information of how much is adsorbed in each step is an important input for unit operation as well as for simulation purposes.

Fig. 3 presents the CO isotherms at temperatures ranging from 279 to 313 K on the different materials. For a better comparison, Fig. 4 was plotted with the isotherms of all samples at 293 K.

All isotherms show typical type I behavior and the experimental data were very well matched by the Toth model (Eq. (6)). The parameters of the Toth isotherm model are summarized in Table 4 for each sample.

The adsorption enthalpy, necessary for the non-isothermal description of the dynamic process, was obtained from the Toth isotherm fitting parameter Q_i, which is equal to the isosteric heat of adsorption, when the fractional loading ($\theta = q_i^*/q_{\max,i}$) is zero [21]:

$$-\Delta H_i\big|_{\theta=0} = Q_i \tag{13}$$

Zeolites clearly show higher adsorption capacities in comparison with the carbon sample for CO (Fig. 4), being the zeolite KÖSTROLITH 5ABF slightly better at pressures above ca. 0.5 MPa. Additionally, the isotherms of zeolites exhibit a more pronounced non-linearity, which has a direct influence on the complexity of a model to simulate adsorptive processes.

The curvature of isotherms plays an important role on the position of the experimental breakthrough time. For linear isotherms and isothermal conditions the breakthrough time should be the same for different concentrations, because the adsorbed amount (loading) and the adsorbate concentration (or partial pressure) increase by the same factor (i.e. constant relationship). Non-linear isotherms, like the ones described by Langmuir or Toth isotherm models, may shift the breakthrough curves to shorter times and the curves become steeper with increasing concentration, for an isothermal case [19,30]. This influence is qualitatively illustrated in Fig. 5 with a theoretical bed of zeolite sample KÖSTROLITH 5ABF, using the respective isotherm fitted parameters as input on the proposed model and keeping all other parameters constant.

From this point on, for the sake of a acceptable model validation, two approaches are generally considered: (i) the non-linear region of the isotherm, i.e. high partial pressures or concentrations, are avoided in the study or (ii) more correlations and parameters are used, increasing the model complexity. On the one hand, operating conditions of practical importance and use for the industry are ignored, and on the other hand the strategy of using more empirical parameters or correlations could be questionable for their validity.

Fig. 6 presents the experimental breakthrough curves and the respective simulations for each sample at the operating conditions listed in Table 3.

A general analysis of the simulations with the proposed model suggests that the predictions were very satisfactory. For most of the cases, however, the breakthrough time is slightly underestimated. This underestimation is more pronounced for the experiments carried out at higher pressures and lower concentrations. This is the case for the zeolites at conditions correspondent to the experimental runs A1, A2, B2, B3, E3, E4, F2, F3 and F4.

The main reason for this small difference on the prediction of the breakthrough time is attributed to the assumption of an adia-

Table 2
Column and bed characteristics.

	Adsorbent sample			
	AC D55/2 C PSA	Zeolite A	Zeolite B	KÖSTROLITH 5ABF
	(C)[a]	(A)[a]	(B)[a]	(E)/(F)[a]
Form	Cylindrical	Spherical	Spherical	Spherical
Bed length [$\times 10^{-2}$ m]	18.2	18.0	18.5	18.2/8.0
Bed mass[b] [$\times 10^{-3}$ kg]	37.03	50.25	50.70	47.35/21.4
Bed porosity	0.38	0.42	0.47	0.45/0.43
Particle porosity	0.44	0.41	0.41	0.41
Average particle radius [$\times 10^{-2}$ m]	0.15	0.1	0.1	0.1
Particle average density [kg m^{-3}]	783	1191	1301	1209
Particle specific heat [J kg^{-1} K^{-1}]	820	920	920	920
Column internal diameter [$\times 10^{-2}$ m]		2.2		
Wall thickness [$\times 10^{-3}$ m]		3		
Wall density [kg m^{-3}]		7860		
Wall specific heat [J kg^{-1} K^{-1}]		477		

[a] Operating conditions.
[b] Non-activated sample – as supplied.

Table 3
Operating conditions of the breakthrough curves experiments and simulations.

Adsorbent: AC D55/2 C PSA	Experimental run		
	C1	C2	C3
Feed temperature [K]	298	299	299
Feed pressure [MPa]	0.50	0.10	1.99
Feed molar fraction of CO [%]	6.6	13.1	13.1
Feed flow rate [cm^3 s^{-1} at SATP]	2.79	2.84	2.84

Adsorbent: zeolite A	Experimental run		
	A1	A2	A3
Feed temperature [K]	296	296	295
Feed pressure [MPa]	2.02	3.98	5.97
Feed molar fraction of CO [%]	17.5	17.5	17.5
Feed flow rate [cm^3 s^{-1} at SATP]	2.99	2.98	2.99

Adsorbent: zeolite B	Experimental run			
	B1	B2	B3	B4
Feed temperature [K]	296	298	293	297
Feed pressure [MPa]	0.10	2.00	3.98	5.98
Feed molar fraction of CO [%]	17.5	17.5	17.5	17.5
Feed flow rate [cm^3 s^{-1} at SATP]	2.99	2.99	2.99	2.98

Adsorbent: KÖSTROLITH 5ABF	Experimental run			
	E1	E2	E3	E4
Feed temperature [K]	301	301	297	300
Feed pressure [MPa]	0.20	0.20	1.00	1.00
Feed molar fraction of CO [%]	5.0	10.0	5.0	10.0
Feed flow rate [cm^3 s^{-1} at SATP]	3.35	3.35	3.35	3.35

Adsorbent: KÖSTROLITH 5ABF	Experimental run			
	F1	F2	F3	F4
Feed temperature [K]	299	300	300	300
Feed pressure [MPa]	0.10	1.99	1.99	3.97
Feed molar fraction of CO [%]	17.5	17.5	9.0	9.0
Feed flow rate [cm^3 s^{-1} at SATP]	2.99	2.99	2.86	2.86

Table 4
Fitting parameters of the Toth model for the adsorbent samples.

Adsorbent	T_0 [K]	$q_{max0,i}$ [mol kg^{-1}]	$K_{0,i}$ [$\times 10$ MPa^{-1}]	$n_{0,i}$	κ_i	χ_i	Q_i [J mol^{-1}]	R^2
AC D55/2 C PSA	298	6.272	0.112	0.662	0.000	0.443	14592	0.9998
Zeolite A	298	7.730	1.974	0.324	0.179	0.000	30463	0.9993
Zeolite B	298	5.815	1.330	0.415	0.177	0.000	31597	0.9995
KÖSTROLITH 5ABF	293	7.584	1.600	0.353	0.083	0.000	26676	0.9997

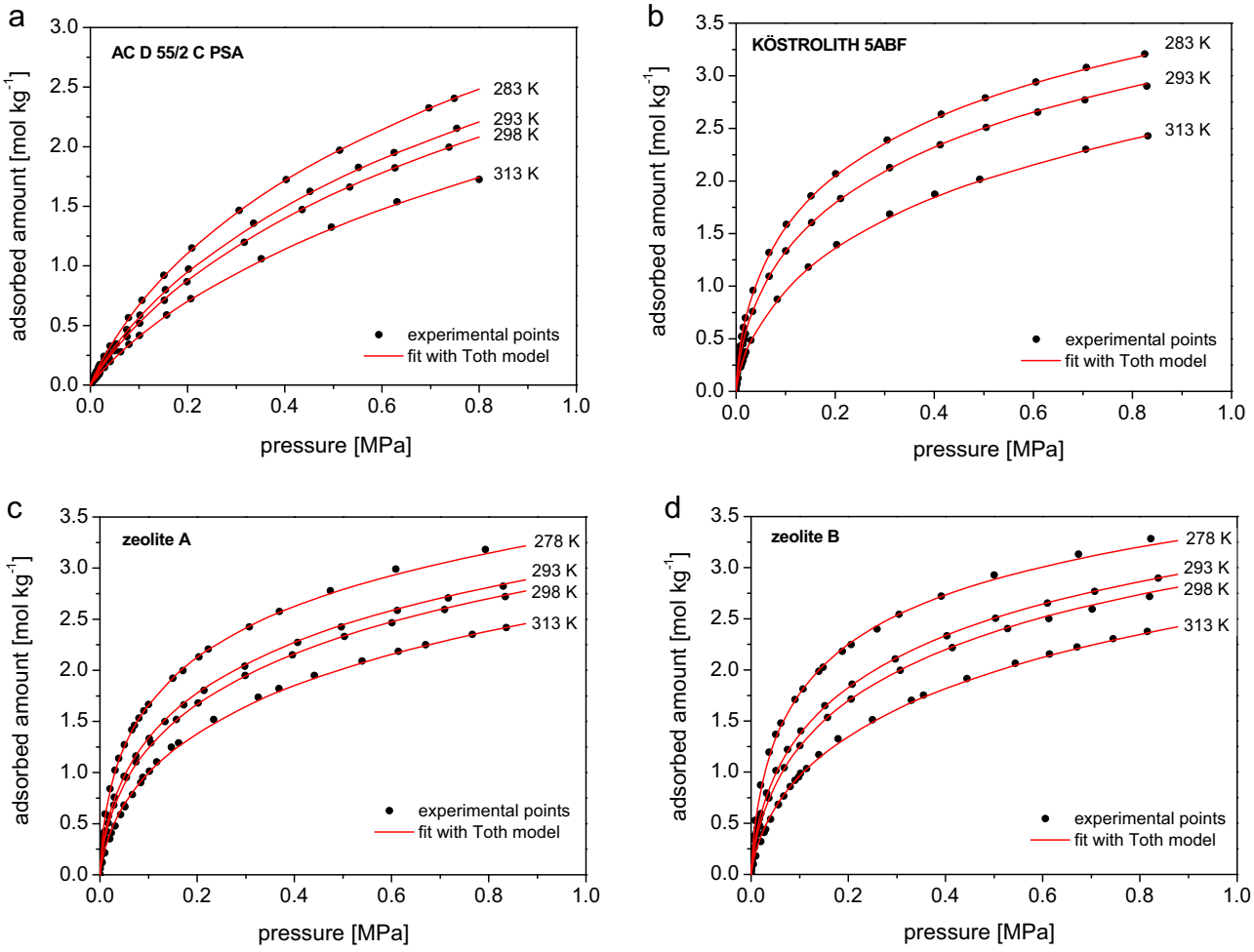

Fig. 3. Isotherms of carbon monoxide on the samples used in the present study.

batic operating condition on the model. Although real adsorptive processes operate near to an adiabatic condition [31], this study made used of a lab-scale fixed bed with dimensions small enough to allow a certain degree of heat transfer to the environment during the experimental runs.

Referring to Table 4, one can observe that the heat of adsorption is significantly higher for the zeolites in comparison with the activated carbon sample. Therefore, the process with zeolites tends to generate more heat, effect which is also proportional to the feed partial pressure. For an adiabatic operation, the system is submitted to a higher temperature increase, which poses a negative impact on the adsorption capacity, dropping the amount of gas (CO) that can be adsorbed, as one can discern from the isotherms in Fig. 3. Consequently, the bed gets saturated faster and CO breaks through the column earlier.

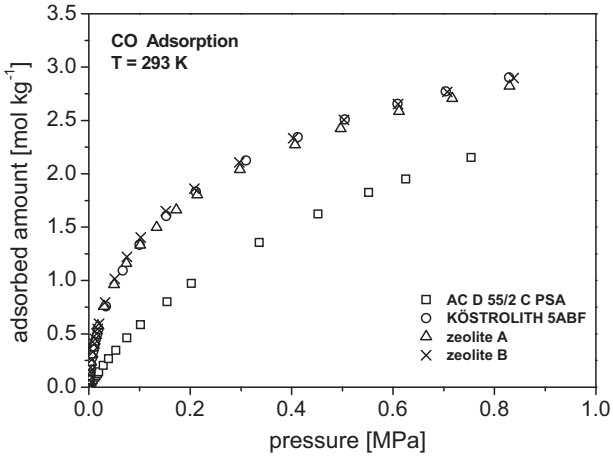

Fig. 4. Comparison of the adsorption capacities of the samples at 293 K.

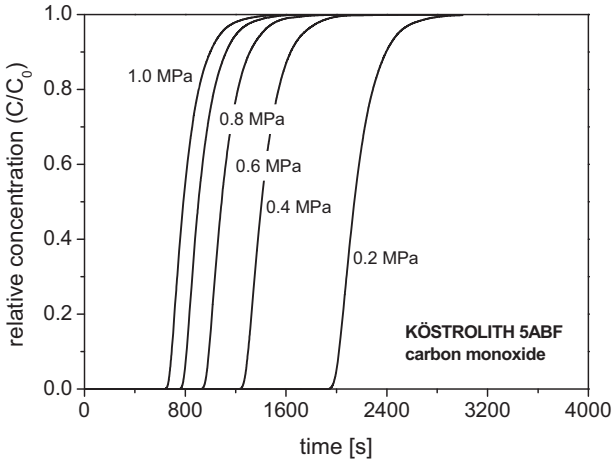

Fig. 5. Influence of the isotherm curvature on the breakthrough time with simulated curves for different feed partial pressures of carbon monoxide.

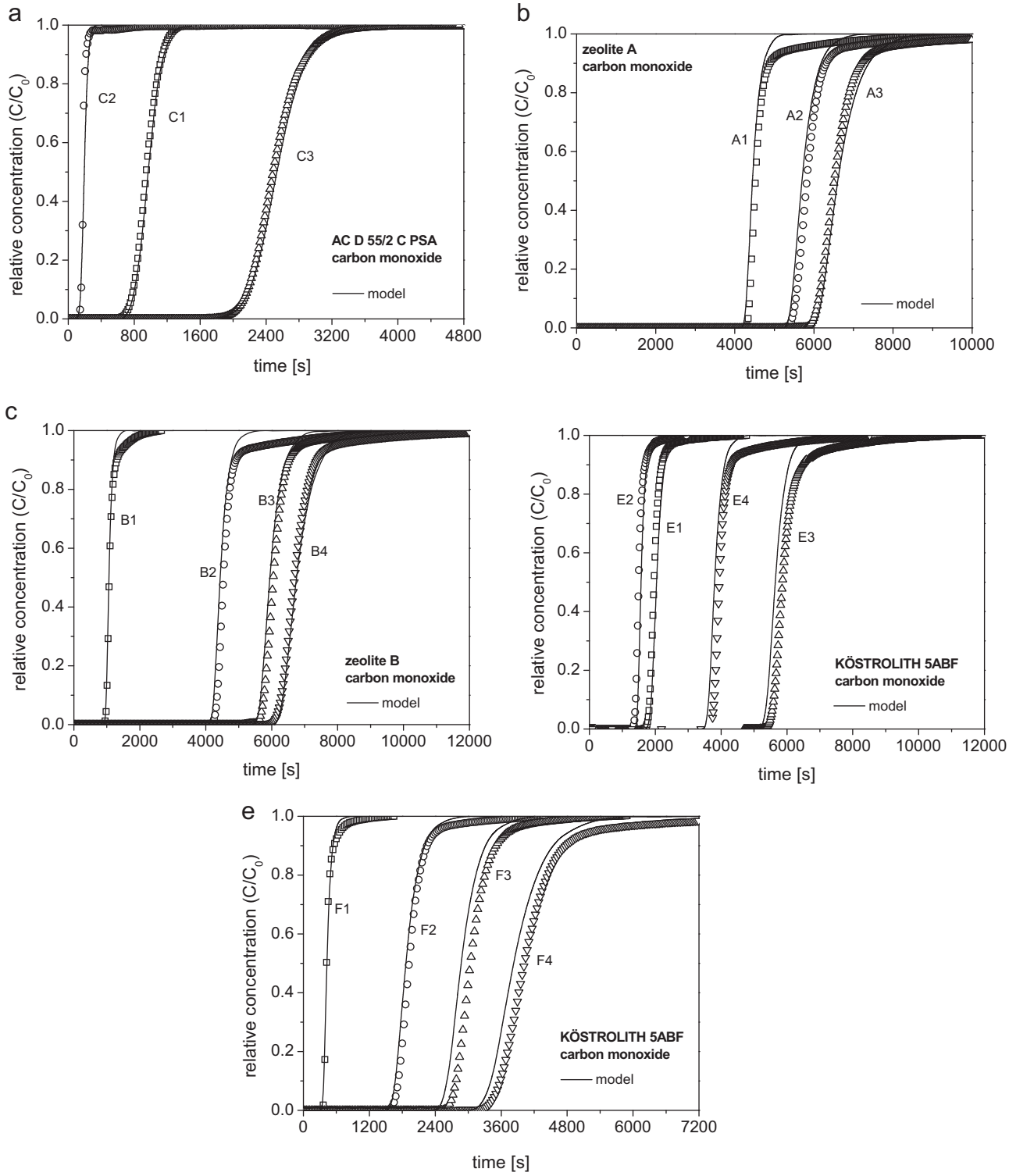

Fig. 6. Breakthrough curves of carbon monoxide on different samples. Points were experimentally obtained and solid lines are simulations with the proposed model. Operating conditions for each curve are listed in Table 3.

In the case of the experiments with activated carbon (C1, C2 and C3), heat should be generated in a lower rate. The same argument is also valid for the cases of B1, E1, E2 and F1, where the feed is much diluted on CO.

To illustrate the heat effects on the temperature increase, Fig. 7 was plotted with the simulated temperature profiles at the column exit for some representative cases, namely C3, F3 and F4. The temperature increases only 2.6 K for the run C3 with the activated carbon. For the operating condition F3 with the zeolite KÖSTROLITH 5ABF, which is even milder than C3 considering the bed height and feed concentration, the temperature increases 8.2 K. For the set of conditions F4 the temperature increase reaches a value of 10.5 K, which is quite considerable to affect the bed adsorptive capacity. As one can observe from the same plot, the simulated temperature rises and remains practically constant since the system is considered to operate adiabatically. Hence, the relative con-

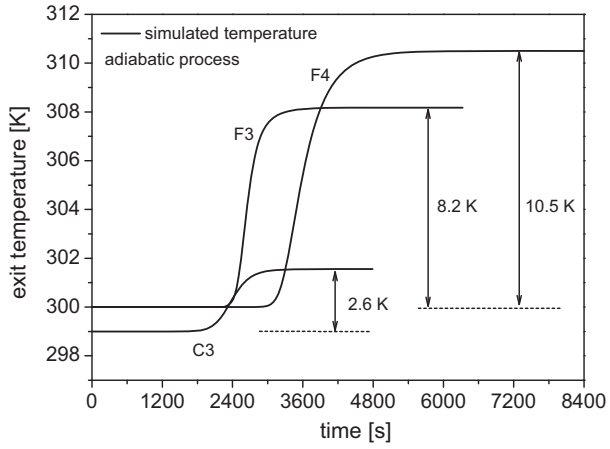

Fig. 7. Comparison of simulated temperature profiles at the column exit for an adiabatic process.

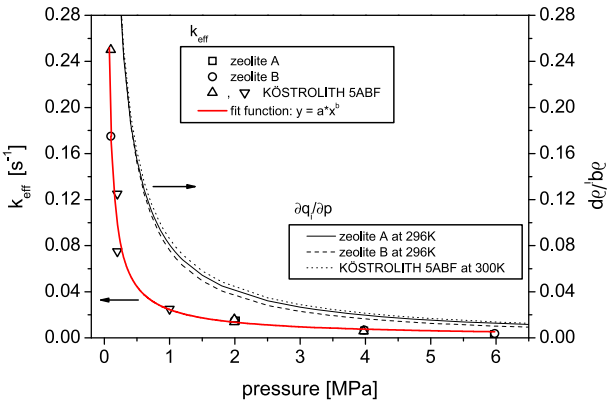

Fig. 8. Trend of the effective mass transfer coefficient in relation to the isotherm curvature along the total pressure.

centration of the simulated breakthrough curves also reaches the unity at the same rate that the temperature reaches the maximum. Unlikely to the experiments, for which it was already observed that heat is transferred to the environment, the temperature reaches a maximum and then starts to decrease and consequently the experimental curves present a slow approach to unity.

Other minor mismatches are also found in the mass transfer zone (MTZ), more specifically on the prediction of the upper region of some breakthrough curves (e.g. A1, A2, B1, B2, B3, E3 and E4). This is likely to be caused by a tailing effect stemmed from the heat of adsorption, which was also observed and discussed in more details in references [32–34]. The deviation between simulation and experimental results may come from the isotherm variation by temperature change and the velocity gap between MTZ and temperature profiles. Additionally, changes on the temperature also lead to changes in the kinetics and such effect was not considered on the model.

The flow rate, influenced by the operating pressure, also plays a role on the process dynamics. What one could also expect from the isotherms in Fig. 3 is that the higher the pressure, the higher CO adsorption and accumulation in the adsorber. Consequently, there could be a misinterpretation of the graphs in Fig. 6. But what actually happens is an indirect influence of the pressure on the retention time, as the volume is compressed reducing the flow speed and increasing the contact time between gas and solid.

The mass flow controllers provide a volume flow under standard conditions. Therefore an increasing of pressure by a known factor would reduce the flow, in an ideal case, also by the same factor. As a consequence, the contact time of solid and gas phases is reduced with increasing pressure. Neglecting the slight differences on the temperature and flow rate, the experiments with zeolite A and zeolite B illustrate the problem.

The mass transport coefficient affects the steepness and the size of the mass transfer zone of a breakthrough curve [7,19]. A faster mass transport (i.e. kinetics) is highly desired for a more efficient use of the adsorbent bed. Regardless of our assumption of constant behavior, this parameter is actually related to the material transport into the pores of the adsorbent, which by itself depends on the concentration gradient, temperature and pressure, and is associated to the curvature of the correspondent isotherm [19]. This association is illustrated in Fig. 8 with the plot of the fitted values of k_{eff}, which are listed in Table 5, along with the isotherm curvature against the total pressure.

Where the curvature is evaluated from Eq. (6) in terms of pressure at finite loadings, according to Ref. [21]:

$$\text{“isoterm curvature”} = \frac{\partial q_i^*}{\partial p} = \frac{K_i q_{\max,i}}{(1+(K_i p)^{n_i})^{(1/n_i+1)}} \quad (14)$$

In Fig. 8, points represent the k_{eff} values, which were connected by means of an empiric exponential decay function of the type $y = ax^b$, and the lines correspond to the isotherm curvature for the zeolites. Although no direct match is found, the purpose of this illustration is to observe the relationship between k_{eff} and $\partial q_i/\partial p$ by the trend shown with the pressure.

The neglect of the pressure drop also seems to be very reasonable for the conditions studied. Despite the common use of an additional equation to describe the pressure drop along the bed, the relative small lengths of the adsorbers in the present study do not seem to be susceptible to significant speed variations due to changes in the total pressure, which is supposed to be controlled by an appropriate device.

If the system experiences pressure drops, it is expected that the flow rate becomes higher and, therefore, the component should earlier breakthrough. No obvious correlation between bed length and the occurrence of considerable pressure drop could be observed in this work.

It is difficult to compare the experimental performance data of H_2/CO separation between the samples studied here because of different operating conditions and system parameters. That the activated carbon presents a less efficient performance in relation to the zeolites is an expected fact, since its adsorption capacity for CO is far lower. But in view of a cyclic process, the cyclic capacities of the samples are fairly comparable, depending on working pressure range, seeing that the shapes of the isotherms are practically identical. The most important factor regarding cyclic capacities is the slope of the isotherm within the working pressure range.

A comparison between the zeolites only is even harder, nevertheless we attempted an evaluation of the performance based on the experimental stoichiometric time corrected with respect to the mass of sample. Similar sets of conditions are desirable for such procedure and therefore we selected A1 for the zeolite A, B2 for the zeolite B and F2 for the KÖSTROLITH 5ABF, which correspond to ca. 2 MPa, ca. 298 K and 17.5% CO in the feed. The time (in s) divided by the sample mass (in g) give us 98.07 for zeolite A, 98.00 for zeolite B and 98.00 for the KÖSTROLITH 5ABF. These results are identical, considering the temperature difference between each set of conditions and experimental deviations, and this is a clear indication that the key for optimizing the performance of H_2/CO separation lies in the adsorption equilibrium, which was presented by the isotherms in advance.

Table 5
Fitted values of the effective mass transport coefficient.

Adsorbent: AC D55/2 C PSA	Experimental run			
	C1	C2	C3	
k_{eff} [s^{-1}]	1.07	2.67	2.67×10^{-2}	
Adsorbent: zeolite A	Experimental run			
	A1	A2	A3	
k_{eff} [s^{-1}]	1.50×10^{-2}	6.25×10^{-3}	3.25×10^{-3}	
Adsorbent: zeolite B	Experimental run			
	B1	B2	B3	B4
k_{eff} [s^{-1}]	1.75×10^{-1}	1.50×10^{-2}	6.75×10^{-3}	3.75×10^{-3}
Adsorbent: KÖSTROLITH 5ABF	Experimental run			
	E1	E2	E3	E4
k_{eff} [s^{-1}]	7.50×10^{-2}	1.25×10^{-1}	2.50×10^{-2}	2.50×10^{-2}
Adsorbent: KÖSTROLITH 5ABF	Experimental run			
	F1	F2	F3	F4
k_{eff} [s^{-1}]	2.50×10^{-1}	1.38×10^{-2}	1.63×10^{-2}	5.75×10^{-3}

5. Conclusion

Breakthrough curves of carbon monoxide were measured on three different 5A zeolites and one activated carbon at different operating conditions. A simple mathematical model was used to simulate the dynamic behavior of the adsorbent bed using inputs of previously measured adsorption isotherms, heat of adsorption and physical properties evaluated according to literature reports.

Despite the simplifications, the model was capable of simulating the breakthrough curves of carbon monoxide with satisfactory agreement with experimental data. In this study, it was observed that the heat effects also play an important role on the evaluation of the breakthrough time. Additionally, the assumption of adiabatic operation appears not to be completely valid, as the simulations of most conditions slightly underestimate the breakthrough time.

The proposed model may be further developed to take into account non-constant flow rates through the bed, pressure drop along the column, temperature dependence of the effective mass transport coefficient in the future. However, it is important to keep in mind that the use of a more sophisticated model requires the knowledge of more parameters as well as their influence on the dynamics of adsorptive processes.

Ideally, every model input should be experimentally attained. But due to experimental limitations such as time, financial aspects or infrastructure, if only some of the model parameters are available from experimental data, one should find other ways to obtain them. That is typically achieved by using correlations but whether they can be properly applied or not is a topic for further discussion.

An important conclusion of this work is that simplified models are capable of properly simulating breakthrough curves under the studied conditions, provided that enough experimental data are available. The indiscriminate use of parameters can lead to an unnecessary model complexity of questionable practical value. Simple models may, however, not properly work for systems with high adsorption and heat effects and considerable derivations from ideal gas behavior like CO_2 rich mixtures.

Acknowledgements

The authors acknowledge the support from INNOWATT - Project Az: IW070135, CNPq (Conselho Nacional de Desenvolvimento Científico e Tecnológico - Brazil), DAAD (Deutscher Akademischer Austausch Dienst - Germany), CarboTech AC GmbH, Mahler AGS GmbH and CWK Chemiewerk Bad Köstritz GmbH. The authors also acknowledge aid of Ulf Roland from the *Zentrum für Umweltforschung* (UFZ – Leipzig, Germany) with sample characterization.

References

[1] D. Simbeck, E. Chang, Hydrogen Supply: Cost Estimate for Hydrogen Pathways – Scoping Analysis, Subcontractor Report, Mountain View, California, 2002, http://www.nrel.gov/docs/fy03osti/32525.pdf (online address).
[2] J. Benemann, Hydrogen biotechnology: progress and prospects, Nat. Biotechnol. 14 (1996) 1101–1103.
[3] D. Das, T.N. Veziroğlu, Hydrogen production by biological processes: a survey of literature, Int. J. Hydrogen Energy 26 (2001) 13–28.
[4] A.M. Ribeiro, C.A. Grande, F.V.S. Lopes, J.M. Loureiro, A.E. Rodrigues, A parametric study of layered bed PSA for hydrogen purification, Chem. Eng. Sci. 63 (2008) 5258–5273.
[5] R.T. Yang, Gas Separation by Adsorption Processes, Imperial College Press, London, 1997.
[6] S. Sircar, T.C. Golden, Purification of hydrogen by pressure swing adsorption, Sep. Sci. Technol. 35 (5) (2000) 667–687.
[7] D.M. Ruthven, Principles of Adsorption and Adsorption Processes, Wiley, New York, 1984.
[8] J.H. Park, J.N. Kim, S.H. Cho, J.D. Kim, R.T. Yang, Adsorber dynamics and optimal design of layered beds for multicomponent gas adsorption, Chem. Eng. Sci. 53 (23) (1998) 3951–3963.
[9] M. Chlendi, D. Tondeur, Dynamic behaviour of layered columns in pressure swing adsorption, Gas Sep. Purif. 9 (4) (1995) 231–242.
[10] S. Cavenati, C.A. Grande, A.E. Rodrigues, Separation of $CH_4/CO_2/N_2$ mixtures by layered pressure swing adsorption for upgrade of natural gas, Chem. Eng. Sci. 61 (2006) 3893–3906.
[11] S. Sircar, Basic research needs for design of adsorptive gas separation processes, Ind. Eng. Chem. Res. 45 (2006) 5435–5448.
[12] Mahler AGS GmbH – Internal Note, 2008.
[13] Chemiewerk Bad Köstritz (CWK) – Internal Note, 2008.
[14] X. Cheng, Z. Shi, N. Glass, L. Zhang, J. Zhang, D. Song, Z.S. Liu, H. Wang, J. Shen, A review of PEM hydrogen fuel cell contamination: impacts, mechanisms, and mitigation, J. Power Sources 165 (2) (2007) 739–756.
[15] C. Tien, Adsorption Calculations and Modeling, Butterworth-Heinemann, Boston, 1994.
[16] D. Bathen, M. Breitbach, Adsorptionstechnik, Springer, Berlin, 2001.
[17] J.A. Delgado, M.A. Uguina, J.R. Sotelo, B. Ruíz, J.M. Gómez, Fixed-bed adsorption of carbon dioxide/methane mixtures on silicalite pellets, Adsorption 12 (2006) 5–18.
[18] S. Karcher, Eignung verschiedener Sorbentien zur Entfernung von Reaktivfarbstoffen aus Abwasser, Dissertation, Technische Universität Berlin, Berlin, 2000 (in German).
[19] W. Kast, Adsorption aus der Gasphase, VCH, Weinheim, 1988.

[20] M. Bastos-Neto, A.E.B. Torres, D.C.S. Azevedo, C.L. Cavalcante Jr., Methane adsorption storage using microporous carbons obtained from coconut shells, Adsorption 11 (2005) 911–915.
[21] D.D. Do, Adsorption Analysis: Equilibria, Kinetics, Series on Chemical Engineering, vol. 2, Imperial College Press, London, 1998.
[22] F.V.S. Lopes, C.A. Grande, A.M. Ribeiro, J.M. Loureiro, O. Evaggelos, V. Nikolakis, A.E. Rodrigues, Adsorption of H_2, CO_2, CH_4, CO, N_2 and H_2O in activated carbon and zeolite for hydrogen production, Sep. Sci. Technol. 44 (2009) 1045–1073.
[23] R.B. Bird, W.E. Stewart, E.N. Lightfoot, Transport Phenomena, revised second ed., Wiley International, New York, 2006.
[24] R.H. Perry, D.W. Green, J.O. Maloney (Eds.), Perry's Chemical Engineers' Handbook, 7th ed., McGraw-Hill, New York, 1999.
[25] F. Dreisbach, H.W. Lösch, P. Harting, Highest pressure adsorption equilibria data: measurement with magnetic suspension balance and analysis with a new adsorbent/adsorbate-volume, Adsorption 8 (2) (2002) 95–109.
[26] A. Herbst, P. Harting, Thermodynamic description of excess isotherms in high-pressure adsorption of methane, argon and nitrogen, Adsorption 8 (2002) 111–123.
[27] F. Dreisbach, R. Staudt, J.U. Keller, High pressure adsorption data of methane, nitrogen, carbon dioxide and their binary and ternary mixtures on activated carbon, Adsorption 5 (1999) 215–227.
[28] R.E. Bazan, M. Bastos-Neto, R. Staudt, H. Papp, D.C.S. Azevedo, C.L. Cavalcante Jr., Adsorption equilibria of natural gas components on activated carbon: pure and mixed gas isotherms, Adsorpt. Sci. Technol. 26 (5) (2008) 323–332.
[29] R. Staudt, S. Bohn, F. Dreisbach, J.U. Keller, Gravimetric and volumetric measurements of helium adsorption equilibria on different porous solids, in: B. McEnaney, et al. (Eds.), Characterization of Porous Solids, vol. 4, Royal Society of Chemistry, London, 1997, pp. 261–266.
[30] M. Bastos-Neto, A. Möller, R. Staudt, J. Böhm, R. Gläser, Breakthrough curves of methane at high pressures for H_2 purification processes, Chem. Ing. Tech., 83 (1–2), doi:10.1002/cite.201000155.
[31] R.T. Yang, P.L. Cen, Improved pressure swing adsorption processes for gas separation: by heat exchange between adsorbers and by using high-heat-capacity inert additives, Ind. Eng. Chem. Proc. Des. Dev. 25 (1) (1986) 54–59.
[32] J.Y. Yang, C.H. Lee, Adsorption dynamics of a layered bed PSA for H-2 recovery from coke oven gas, AIChE J. 44 (1998) 1325–1334.
[33] J.G. Jee, M.B. Kim, C.H. Lee, Adsorption characteristics of hydrogen mixtures in a layered bed: binary, ternary, and five-component mixtures, Ind. Eng. Chem. Res. 40 (2001) 868–878.
[34] J.J. Lee, M.K. Kim, D.G. Lee, H. Ahn, M.J. Kim, C.H. Lee, Heat-exchange pressure swing adsorption process for hydrogen separation, AIChE J. 54 (2008) 2054–2064.